Soft Matter

PAPER

View Article Online
View Journal | View Issue

Cite this: *Soft Matter*, 2018, **14**, 9475

Influence of protein charge patches on the structure of protein–polyelectrolyte complexes†

Rituparna Samanta and Venkat Ganesan *

Received 27th July 2018,
Accepted 29th October 2018

DOI: 10.1039/c8sm01535j

rsc.li/soft-matter-journal

We employ a combination of the single chain in mean field simulation approach with the solution of Poisson's equation to study the influence of charge heterogeneities on the structure of protein–polyelectrolyte complexes. By adopting a coarse-grained model of representing proteins as charged nanoparticles, we studied the influence of the pattern of charge heterogeneities, net charge, ratio of positive to negative charges on the patches, and the volume fraction of the particles on the structural and aggregation characteristics of proteins in polyelectrolyte solutions. Our results demonstrate that the pattern of charge heterogeneities can exert a significant influence on the resulting characteristics of the aggregates, in some cases leading to a transformation from polymer-bridged complexes into direct particle aggregates driven by the attraction between oppositely charged patches.

1 Introduction

Mixtures of proteins and polyelectrolytes are widely used in food systems to modulate the structure, texture and stability of food through the resulting thickening and gelling characteristics.[1] Further, protein–polyelectrolyte complexes are also often utilized in applications such as enzyme immobilization,[2,3] DNA delivery,[4] design and production of biomaterials for cell micropatterning[5] and separation of proteins.[6–9] In such contexts, mixtures of proteins and polyelectrolytes are commonly observed to phase-separate by one of two means: when the interaction between the protein and polyelectrolytes is repulsive with respect to inter-protein or inter-polyelectrolyte interactions, they separate into phases enriched respectively by each of the components. The phase separation resulting in such cases is known as the segregated phase separation. In contrast, when the proteins and polyelectrolytes have an attractive interaction (either of electrostatic or enthalpic origin), two types of phase behavior have been observed: (a) liquid–liquid (coacervate) phase separation; and (b) solid–liquid (precipitate) phase separation.[10,11] Despite the lack of a clear demarcation between the latter categories, it is generally understood that both modes of phase separation result in turbid solutions distinguished by the formation of spherical droplets (liquid–liquid) as opposed to amorphous solid particles (solid–liquid).[12–15]

There has been a significant number of experimental studies aimed at understanding the physics and parameters underlying the structural characteristics and the phase behavior of protein–polyelectrolyte mixtures.[13,16] Such studies have demonstrated that the interactions and the resulting phase behavior of protein–polyelectrolyte mixtures can be influenced by a variety of factors such as the charge of the individual entities, solution conditions, geometry of the globular proteins and temperature.[1,13,16] Since the accompanying parameter space is extremely vast, there have also been a few simulation studies which have probed the influence of different protein and polyelectrolyte characteristics on the resulting phase behavior.[17–21]

While the above studies have yielded useful insights, a common assumption underlying many of the models used in simulations or in interpreting experiments has been that the proteins possess a fixed charge which is uniformly distributed over their surface or volume. However, in reality, proteins often exhibit heterogeneous charge patches arising from the distribution of different chemical groups on the solvent exposed surface.[6,22–25] Moreover, such charge heterogeneities can also result from the partial dissociation and acid–base equilibria arising under different solution conditions (pH). A number of recent experiments have hinted at the possible nontrivial influence of such protein charge heterogeneities on protein–polyelectrolyte complexation characteristics. For instance, Harnsilawat *et al.*[26] studied the complexation of β-lactoglobulin (protein) and alginate (polyanion), and showed that the polyanions formed complexes with the protein even at the isoelectric point of the latter. Mattison *et al.*[27] have similarly demonstrated the formation of soluble complexes between globular protein BSA and polycation poly-(dimethyldiallylammonium chloride) (PDMDAAC) even when the net charge of the protein was positive. A number of other experiments have demonstrated the formation of complexes under the conditions when the net charge of the protein was of the same sign as that of the polyelectrolyte.[6,28–31]

Department of Chemical Engineering, University of Texas at Austin, Austin, Texas 78712, USA. E-mail: venkat@che.utexas.edu

† Electronic supplementary information (ESI) available. See DOI: 10.1039/c8sm01535j

Such experiments have commonly been interpreted as a consequence of the complexation between local patches on the protein of opposite charge to that of the polyelectrolyte.

To our knowledge, there has been no prior theoretical study on the influence of charge heterogeneities on the structure and phase behavior of protein–polyelectrolyte mixtures. Seminal studies by deVries[32,33] and Ellis *et al.*[34] have probed the influence of charge patches on the adsorption of polyelectrolytes, and have identified the physics underlying adsorption under conditions of the same sign of net charge of the protein and the polyelectrolytes. However, such studies pertain to a single surface/protein and do not address the physics resulting in multiple protein systems. In a different context, a number of recent studies have been concerned with the self-assembly and phase behavior of "patchy" particles.[35–44] Many such studies were concerned with "patchiness" arising from enthalpic interactions rather than in electrostatic features.[36,39–41] While recent work by Bianchi *et al.*[38,42–44] considered the interparticle interactions arising due to charged patches, such studies however do not address the physics arising from the presence of charged polyelectrolytes and the structure of complexes resulting as a consequence of polymer–protein interactions.

In this study, we take the first steps to address the influence of protein surface charge heterogeneities on the phase behavior and complexation characteristics of charged protein–polyelectrolyte mixtures. Towards such an objective, we consider a model in which the globular proteins are represented as spherical nanoparticles and implement a simple model for studying the influence of charge heterogeneities. Real proteins render random distribution of charges which are dependent on the solution conditions. However, as a first step towards such complex charge distributions, in this work we have used toy models with regular charge distributions (details will be discussed in Section 2). We believe that the insights resulting from the systematic study of such simpler models could also be potentially useful for efforts aiming to engineer the charge distribution of proteins to achieve the desired structure and properties of protein polyelectrolyte complexes.[45]

In the context of the above model, we adapt recent methodological developments from our group in which a variant of the single chain in mean field (SCMF) simulation approach has been used to study the complexation behavior in mixtures of uniformly charged proteins and polyelectrolytes. One of the main advantages of this approach is that it avoids any assumption of "effective" particle–particle interactions and dependences based on the concentration of proteins or polyelectrolytes. Using such a methodology, we clarify the influence of protein charge heterogeneities on the structure, the cluster size distributions of resulting aggregates for multiple proteins and multiple polyelectrolyte systems. Together, our results suggest a nontrivial influence of charge patches on the resulting complexation characteristics.

The rest of the article is organized as follows. In Section 2, we discuss the model details underlying the simulation methodology used in this study. In Section 3, we discuss the parameters and numerical methodologies used for the simulation framework. In Section 4 we present the simulation results. Therein, we first present the characteristics of adsorption and bridging of polyelectrolytes on heterogeneously charged proteins. Subsequently, we present the results for the structural characteristics of mixtures of polyanions and heterogeneously charged proteins. Specifically, we consider two distinct cases: (a) polyampholyte proteins with a net positive charge; and (b) polyampholyte proteins with a net negative charge. We conclude the article with a summary of results and findings in Section 5.

2 Model description

In this work, we focus on globular proteins, and adopt a simple model of (charged) spherical nanoparticles to model such entities. To acknowledge such a model simplification, hereafter, we refer to the protein interchangeably as charged particles. Moreover, real proteins are likely to embody complex physics in which the positive, negative and neutral charge patches are distributed in a manner which correlates with the underlying sequence and the solution conditions. To render progress towards such problems, we advance a simple "toy" model in which the charge heterogeneities are represented as charge patches distributed on the surface sections defined by an angle α (shown in Fig. 1). We use the term "number of patches" to denote the number of regions on which there are positive charges. The net positive charge (distributed uniformly over all patches) is denoted as Q_p. The rest of the particle surface is either neutral or has a negative charge Q_n. The net charge of the particle is denoted as $Q_{\text{net}} = Q_p - Q_n$. The nomenclature "PIn" is used to refer to the geometric variants that contain "n" patches of negative (or neutral) charges.

We classify the patchy particles in terms of the magnitude of charge patches as (a) non-polyampholyte particles: containing only positively charged patches, with the other patches being neutral ($Q_p \neq 0$, $Q_n = 0$); (b) positive-polyampholyte particles: containing both positive and negatively charged patches, such that the net charge is positive ($Q_{\text{net}} > 0$); (c) negative-polyampholyte particles: containing both positive and negative

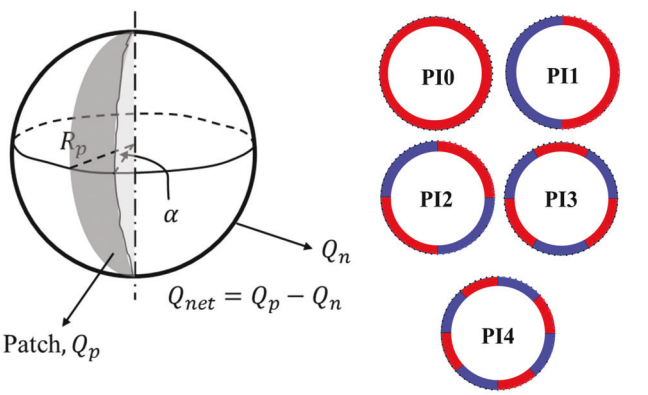

Fig. 1 Model of patchy particles. The red color shows patches of positive charge, and the blue color depicts negative or neutral patches.

patches charged such that the net charge is negative ($Q_{net} < 0$). In the spirit of maintaining simplicity as a first study, for all the charged entities we assume fixed charges which are invariant to changes in solution conditions. The representative models of patchy particles used in our study are depicted in Fig. 1.

We consider a system of N_p heterogeneously charged spherical particles of radius R_p and n negatively charged polymer chains of m monomers each and radius of gyration R_g in a periodic cubic box of volume V. To maintain the overall electroneutrality of the system, n_p and n_m point counterions for the particles and polymers are also included. In this work, we did not consider the influence of additional salt. Hereafter, the concentration of the polymer is presented in units of the overlap concentration C^* of an ideal linear polymer chain solution. The charge on the monomers of the polymer is denoted as z_m. The volume fraction of the particles is denoted as ϕ_p. We assume the dielectric constant of the particle to be the same as that of the solvent.

We assume a flexible chain model for the polyelectrolytes, in which the intramolecular interactions in the polymer chains are modeled through a bead spring model, with bonded Hookean interactions between the beads:

$$\frac{H_b}{k_B T} = \frac{3}{2b^2}\sum_{i=1}^{n}\sum_{s=1}^{m-1}[\mathbf{r}_i(s) - \mathbf{r}_i(s+1)]^2, \tag{1}$$

where $\mathbf{r}_i(s)$ represents the coordinate of the sth bead on the ith polymer. Excluded volume interactions between the polymer segments are incorporated through a simplistic implicit solvent interaction potential of the form:

$$\frac{\bar{u}(\mathbf{r})}{k_B T} = u_0\delta(\mathbf{r}), \tag{2}$$

where u_0 is commonly known as the excluded volume parameter.[46] In the above framework, the non-bonded interactions between the polymer segments can be formally recast as:

$$\frac{H_s}{k_B T} = \frac{u_0}{2}\int \hat{\rho}_{poly}{}^2(\mathbf{r})\mathrm{d}\mathbf{r} \tag{3}$$

where $\hat{\rho}_{poly}$ is the microscopic polymer segment density,[47]

$$\hat{\rho}_{poly}(\mathbf{r}) = \sum_{i=1}^{n}\sum_{s=1}^{m}\delta[\mathbf{r} - \mathbf{r}_i(s)]. \tag{4}$$

The instantaneous density of particles is similarly quantified through a particle volume fraction field as:

$$\rho_{part}(\mathbf{r}) = \sum_{i=1}^{N_p}\int_{r_i}^{r_i+R_p}\hat{\rho}_{part}(\mathbf{r})h\left(\left|\mathbf{r}' - \mathbf{r}_i'\right|\right)\mathrm{d}\mathbf{r}', \tag{5}$$

where $\hat{\rho}_{part}(\mathbf{r}) = \delta(\mathbf{r} - \mathbf{r}_i)$ and $h(r) = 1$ when $|r| < R_p$. The counterions were considered to be point charges and their microscopic densities are given by:

$$\begin{aligned}\rho_{mi}(\mathbf{r}) &= \sum_{i=1}^{n_m}\delta(\mathbf{r} - \mathbf{r}_i)\\ \rho_{pi}(\mathbf{r}) &= \sum_{i=1}^{n_p}\delta(\mathbf{r} - \mathbf{r}_i).\end{aligned} \tag{6}$$

For modeling particle–counterion and particle–monomer interactions, the particles are envisioned as spherical objects with a thin layer of penetrable soft core surrounding an impenetrable hard core. The repulsive interactions between the particle and the polymer monomers/counterions are modeled through a potential of the form:

$$W_{cp}(\mathbf{r}) = 50\left[1 - \tanh\left(2\frac{\mathbf{r} - \alpha R_p}{\beta}\right)\right]k_B T. \tag{7}$$

The coefficients α, β control the steepness and range over which the repulsive potential decays from 100 $k_B T$ to 0 $k_B T$. We have used $\alpha = 0.9$ and $\beta = 0.5$ for the simulation, which ensures that the particle cores are almost impenetrable to counterions and polymers.

The direct interparticle interactions are modeled through a hard-sphere interaction:

$$\frac{H_{pp}}{k_B T} = \frac{1}{2}\sum_{i=1}^{N_p}\sum_{j=1(j\neq i)}^{N_p}U_{HS}\left(|\mathbf{r}_i - \mathbf{r}_j|\right), \tag{8}$$

where

$$U_{HS}(r) = \begin{cases}0, & \text{if} \quad r \geq 2R_p\\ \infty, & \text{if} \quad r < 2R_p\end{cases}. \tag{9}$$

For the simulations of the structure of protein–polyanion mixtures, we have used the Single Chain in Mean Field (SCMF) approach introduced by Mueller and coworkers.[20,48–51] In the SCMF framework, the non-bonded pair-wise interactions are replaced with fluctuating potential fields which are conjugate to the corresponding density fields.[48] The electrostatic energy arising from the charges is represented in terms of its conjugate electrostatic potential field $\varphi(\mathbf{r})$ and the associated energy:

$$\frac{H_{el}}{k_B T} = \int \mathrm{d}\mathbf{r}\left[\rho_e(\mathbf{r})\varphi(\mathbf{r}) - \frac{1}{8\pi l_b}|\nabla\varphi(\mathbf{r})|^2\right], \tag{10}$$

where $\rho_e(\mathbf{r})$ is the total charge density arising from particles, polymers and counterions (in units of e), and is given as:

$$\rho_e(\mathbf{r}) = z_{part}(\mathbf{r})\rho_{part}(\mathbf{r}) \pm \sum_{ion} z_{ion}\rho_{ion}(\mathbf{r}) - z_m\hat{\rho}_{poly}(\mathbf{r}), \tag{11}$$

where z_{ion} is the valency of each ion (co- or counterions), $z_{part}(\mathbf{r})$ is the local fractional charge of the particle, which in turn depends on the sign and magnitude of the particle patch at $\mathbf{r}$. The field $\rho_{ion}(\mathbf{r})$ denotes the local density of co- and counterions. The electrostatic potential $\varphi(\mathbf{r})$, in units of $k_B T/e$, is obtained as the solution of Poisson's equation:

$$\nabla^2\varphi(\mathbf{r}) = -4\pi l_b\rho_e(\mathbf{r}) \tag{12}$$

In the above equation, l_b is the Bjerrum length, defined as $e^2/4\pi\varepsilon_0\varepsilon_r k_B T$, where ε_r is the relative dielectric constant of the medium and ε_0 is the vacuum permittivity. For water, at 300 K, $l_b \approx 0.7$ nm.

To embed our model for particle charge heterogeneities within a grid-like representation of the SCMF approach, we divided the surface of each sphere into grids and distributed the charges uniformly such that all the grid points covering the positive charge patch have a fractional charge totaling Q_p and the grid points covering the negative charge patch have a fractional charge totaling Q_n.

3 Numerical methods and parameters

The model described in the previous section is used in a Monte Carlo simulation approach in which the configuration space is sampled using the Metropolis algorithm.[52] We began the simulation by placing the particles in a cubic lattice configuration and the polymers and the counterions randomly in the rest of the space. In the initial portion of the simulation, 10^4 Monte Carlo (MC) moves are effected such that only the polymers are moved while keeping the particles fixed in space. This pre-equilibration is done to ensure removal of any particle–polymer overlaps. Subsequently, each Monte Carlo step (MCS) involves a MC move for all particles, a slithering snake move for all polymer chains and 100 MC moves for all polymers and counterions. Every MC move of the particle includes a translation and rotation move for all particles. Using such a sequence of moves, the system is equilibrated for 5×10^4 MCS. Subsequently, the properties are averaged over 5×10^4 MCS, constituting the production cycle. Using the position of the monomers, particles and ions, the density fields, charge density fields and electrostatic fields are updated after every move of the polymer and particles.

We use a Fast Fourier Transform (FFT) based numerical method to solve the Poisson equation (eqn (12)).[20,51,53–55] For our study, we have used the Bjerrum length (l_b) as 0.7 nm, corresponding to that of water at 300 K. In this study we have kept the value of $u_0 = 10$, representing a good solvent. We note that, previous studies from our group suggested that excluded volume interactions exert only a small influence on the results.[20,51] The particles used in the simulation are of radii $R_p = 10$ nm and the homopolymers are of $R_g = 24$ nm. For the simulation, we have used a periodic cubic box of size $(200\text{ nm})^3 \approx 20R_p \times 20R_p \times 20R_p$ divided into $64 \times 64 \times 64$ grids. In this study, we did not probe the effect of varying R_p or R_g.

4 Results and discussion

In a recent study from our group,[20] we considered the structural characteristics of uniformly charged spherical nanoparticles in an oppositely charged polymer solution. In such a context, we demonstrated that there are broadly two categories of structural characteristics accompanying mixtures of charged particles and oppositely charged polymers. Explicitly, under conditions of low charges of the particle and/or high polymer concentrations, the depletion interactions introduced by the polymer solution dominate both electrostatic repulsion between the particles and the electrostatic attraction between the polymers and the particles. For such conditions, the particles exhibited aggregation (termed as ''particle–particle aggregates'') arising from the short-ranged depletion attraction. In general, higher particle volume fractions led to screening of interparticle electrostatic repulsions and enhanced the propensity for formation of such direct particle aggregates. In contrast, under conditions of high polymer and particle charges, and at dilute polymer concentrations, polymer-bridged particle complexes were shown to result. Such structures were most clearly evident in the particle–particle radial distribution functions as a peak at a distance shifted from the particle contact.

In the present study, we are mainly concerned with the regimes corresponding to polymer-bridged particle complexes (coacervates), which prove to be of interest for a number of applications.[2,3,6–9] Further, to focus specifically on the influence of particle charge heterogeneity (and to limit the number of parameters), we fixed the polymer concentration C/C^* and polymer charge Q_{pol}, and only probed the role of the particle charge, volume fraction of particles and the characteristics of charge heterogeneities. Specifically, in this work we fixed $C/C^* = 0.092$, $Q_{pol} = 120$, which correspond to parameters which led to the formation of polymer-bridged structures with homogeneous charged particles.[20]

Before delving deeper into the structure of multiparticle systems, we investigated the effect of protein charge heterogeneities on the adsorption and the bridging characteristics of polyelectrolytes. Of specific interest in this context was the case of negative-polyampholyte particles, and to identify conditions in which net polymer adsorption and bridging can result despite the like-charged nature of the polyelectrolytes. To maintain brevity, we restrict most of the results and discussion in such a context to the models ''PI1'' and ''PI2''.

4.1 Influence of particle charge heterogeneities on polymer adsorption

To quantify the influence of protein charge heterogeneities on the adsorption characteristics of the polyanion, a single charged particle was placed in the center of the simulation box and the polymers and the counterions were allowed to equilibrate The net adsorption of polymers was quantified as follows:

$$\text{Net adsorption} = \int_{R_p}^{\infty} d^3\mathbf{r}\left(\rho_{pol}(\mathbf{r}) - \rho_{avg}\right) \qquad (13)$$

where $\rho_{pol}(\mathbf{r})$ and ρ_{avg} denote the local and bulk polymer concentrations respectively.

The results displayed in Fig. 2(a) depict the effect of the particle charge Q_{net} on the net polymer adsorption for non-polyampholyte PI0, PI1 and PI2 particles ($Q_p = Q_{net}$; $Q_n = 0$). As expected, for all the geometries, the net adsorption of polymers increases with an increase in Q_p due to the enhanced attraction between the polyanions and the positive patches of the particle. For uncharged particles ($Q_{net} = 0$), the net adsorption is

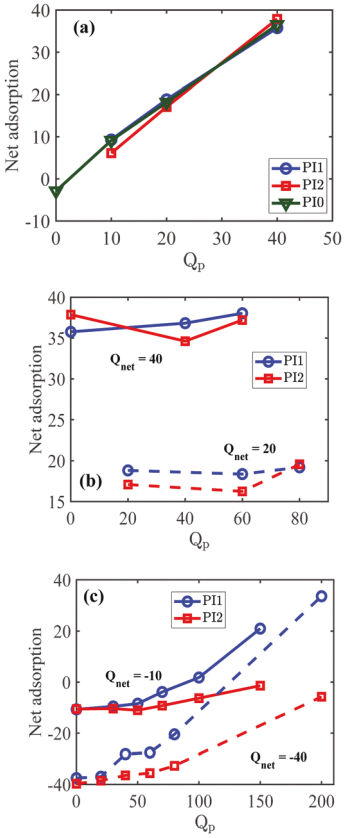

Fig. 2 Net adsorption for (a) non-polyampholyte particles with net charge Q_{net}; (b) positive-polyampholyte particles with net charge Q_{net} = 20 (dashed lines), 40 (solid lines); and (c) negative-polyampholyte particles with net charge Q_{net} = −10 (solid lines), −40 (dashed lines).

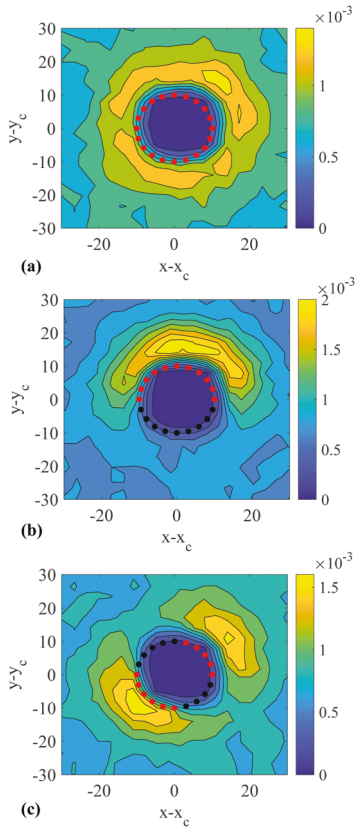

Fig. 3 Polymer concentration around non-polyampholyte particles: (a) PI0, Q_p = 20; (b) PI1, Q_p = 20, Q_n = 0; and (c) PI2, Q_p = 20, Q_n = 0 particles. The red dots indicate regions of positive surface charge, and the black dots correspond to the neutral portions. x_c, y_c denotes the x- and y-coordinates of the center of the box which coincides with the center of the particle.

negative due to the depletion of polymers resulting from entropic exclusion from particle interiors. Interestingly, for non-polyampholyte particles, the adsorption of polymers is seen to be almost insensitive to the heterogeneity of charge distribution. Such a result can be rationalized by using the 2-D polymer concentration profile around the particle presented in Fig. 3. Therein, it can be seen that for PI1 and PI2 particles, despite the greater local concentration of polymers near the positively charged patches (as a consequence of the higher magnitude of the charge on the patch), the polymers are depleted near the uncharged patch of the particle, which leads to similar "net adsorption" to that of the PI0 particles.

The results presented in Fig. 2(b) and (c) display the effect of Q_p on the net polymer adsorption on *polyampholyte* particles with net charge Q_{net}. For polyampholyte particles, there is also expected to be adsorption of polyanions to the positively charged part of the particle and a depletion from the negatively charged patches of the particle. However, in contrast to the non-polyampholyte particles, polymer depletion in polyampholyte particles is expected to reflect a combination of both electrostatic repulsions between the polymer and the negative charge patches and the exclusion of the polymer from the particle interior. Such expectations are seen to be borne in the polymer concentration profiles displayed in Fig. 4(a and b).

For positive-polyampholyte particles (Fig. 2(b)), the net adsorption is seen to be always positive and increases with an increase in Q_p. However, for negative-polyampholyte particles (Fig. 2(c)), we observe an interesting behavior in which the net polymer adsorption crosses over from being negative at small Q_p to a positive value at larger Q_p. These results, which are similar to the results seen in earlier studies by deVries[32,33] and Ellis *et al.*,[34] can be understood as arising from the adsorption of polymers on the positively charged patches compensating for the depletion around the negatively charged patches (Fig. 4(c and d)). As may be intuitively expected, if the difference in the charges of the positive and negative patches is smaller (Q_{net} = −10), a smaller value of positive charge is required to overcome the depletion from the negative patches.

For both the positive and negative polyampholyte cases, the net adsorption for PI2 particles is seen to be lower than that for PI1. Such a result can be understood as a consequence of two factors: (i) the magnitude of charge of the individual patches is lower in PI2 systems compared to PI1. Hence, the driving force for adsorption on oppositely charged patches is correspondingly reduced for PI2 particles; (ii) the positive and negative patches are located in closer proximity in PI2 particles as compared to PI1 particles. Hence, there is an increased repulsion between the negative charge patches and the polymers

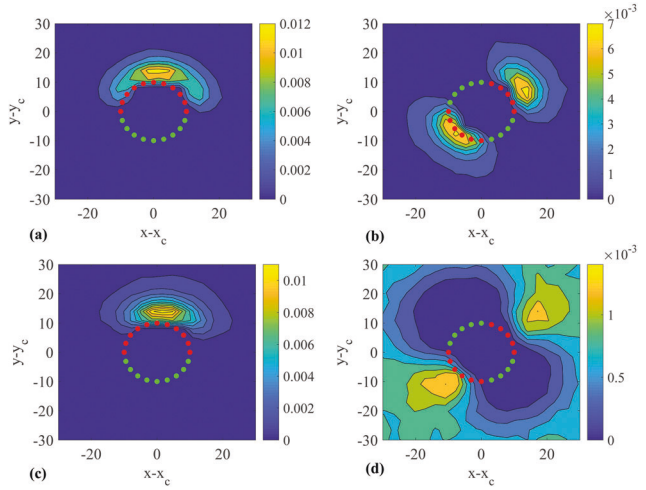

Fig. 4 Polymer concentration around polyampholyte particles: (a) PI1, Q_p = 80, Q_n = 40; (b) PI2, Q_p = 80, Q_n = 40; (c) PI1, Q_p = 80, Q_n = 120; (d) PI2, Q_p = 80, Q_n = 120. The red dots indicate regions of positive surface charge, and the green dots correspond to the negative surface charge. x_c, y_c denotes the x- and y-coordinates of the center of the box which coincides with the center of the particle.

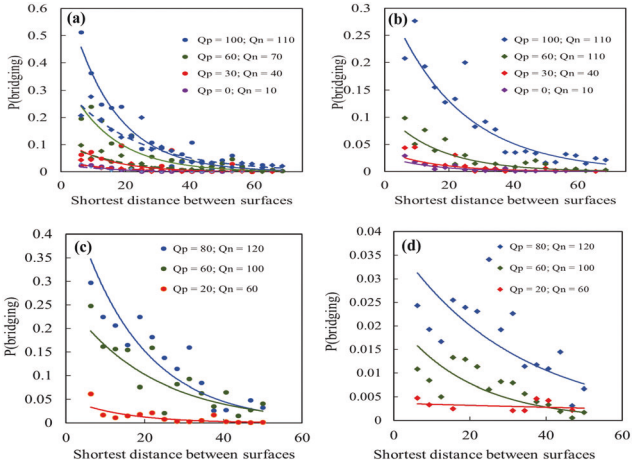

Fig. 5 Probability of bridging as a function of distance between the particle surfaces for negative polyampholyte particles: (a) PI1 particle with Q_{net} = −10; (b) PI2 particles with Q_{net} = −10. (c) PI1 particles with Q_{net} = −40; (d) PI2 particles with Q_{net} = −40. The solid lines are exponential best fits to the data points based on the square of error minimization.

in PI2 particles, which contributes to an enhanced depletion for the negatively charged particles.

4.2 Bridging characteristics in negative-polyampholyte particles

As a complement to the results for polymer adsorption presented in the previous section, we also studied the polymer bridging characteristics accompanying particles with charge heterogeneities. Explicitly, we set out to quantify the probability of forming a polymer bridge, defined as the ratio of average number of polymers forming bridges between two particles to the average number of polymers adsorbed on the first particle. To quantify the bridging characteristics, we considered a two particle system in which one of the particles was fixed in the center of the box and the second particle at a certain distance r from the center of the first particle. After the pre-equilibration steps, the number of bridged polymers relative to the number adsorbed is calculated. However, as a consequence of the fact that both the central particle and the satellite particle possess charge heterogeneities, we also perform rotation and revolution moves to span the solid angle coordinates of both the particles. Understandably, such calculations are computationally expensive and the statistics was poor. Hence, we restrict our results and discussion only to the case of negative-polyampholyte particles.

Fig. 5(a–d) present the results for the probability of bridging for polyampholyte particles with Q_{net} = −10 and −40. As expected, due to the accompanying entropic costs, the bridging probability decreases with an increase in distance between the two particles. More interestingly, due to the adsorption of polymers on the oppositely charged patches of the two particles, we observe that the probability of bridging is non-zero even when the net charge of the particles is negative. At a particular distance r, the probability of bridging increases with an increase in Q_p which can be attributed to an increase in the adsorption of the negatively charged polymer on the positive patches (*cf.* Fig. 2(c)). The probability of bridging for PI2 is lower than that for PI1, which is commensurate with the respective adsorption characteristics and discussion presented in Fig. 2(c).

In summary, the results presented in the previous and the present section demonstrate that the net adsorption and bridging characteristics of polymers around the charged particles depend upon the magnitude of the charge patches as well as the characteristic of the charge distribution. The net adsorption for non-polyampholyte particles was seen to increase with an increase in Q_p, but was almost invariant to the heterogeneity of charge distribution. For positively charged polyampholyte particles, the net adsorption was seen to be positive. However, for the negatively charged polyampholyte particles, the net adsorption was negative for smaller Q_p, but became positive for larger Q_p. Correspondingly, we observed nonzero probabilities for forming polymer bridges between the negatively charged polyampholyte particles. For such cases however, the net adsorption and the bridging probabilities for PI2 were seen to be lower than those for PI1. Together, such results provide an indication of the physics likely to accompany the phase behavior of mixtures of such heterogeneously charged nanoparticles and polyanions. In the following sections, we present results which explicitly quantify the structural characteristics of such multi-particle systems.

4.3 Quantification of the structure of particle aggregates and particle–polymer complexes

For systems of mixtures of (multiple) charged particles and polymers, we quantified our results through three measures of the particle structure: (i) particle–particle radial distribution functions (RDF); (ii) cluster size distributions of direct particle aggregates and particle–polymer complexes

(*i.e.* polymer-bridged particle aggregates); and (iii) bridging fraction (B_r), representing the number of polymers forming polymer bridges relative to the total number of polymers in the system. In this section, we describe briefly the framework adopted to quantify these measures.

The particle–particle RDFs provide a convenient "first-pass" approach to distinguish solution conditions leading to direct particle aggregation from those which lead to polymer-bridged particle complexes. Specifically, RDFs characterized by a peak shifted from the surface of the particle by a distance $\sim R_g$ are classified as polymer-bridged aggregates (PB). In contrast, when there is a peak in the RDF near the surface of the particle (albeit, as will be discussed later, such a peak can manifest shifted from the surface of the particle), such states are classified as direct particle aggregates (PP). Cases in which a peak in the value of RDF was observed both at the particle contact and at a shifted distance are termed as a mixed phase (PP + PB). We note that we did not impose any critical value for the magnitude of the peak in the RDF to identify the different states.

As will be seen in our results discussed later, the particle–particle RDF alone does not allow us to distinguish direct particle aggregates from polymer bridged aggregates. The SCMF framework uses an explicit representation of polymers and particles (in contrast to other approaches which are similar in spirit)[54,56–58] and is hence especially advantageous for further quantification of the characteristics of the aggregates. Towards such objectives, we used a procedure proposed by Sevick *et al.*[20,51,59–62] and adapted in our earlier work in which "clusters" (both particle–particle and particle–polymer) are mapped onto a connectivity matrix. By identifying the indirect contacts arising within the matrix, statistics of the unique clusters can be delineated. We consider all the particles in the system while constructing the cluster size distribution. In our work, particles were considered to be in contact when the distance between two particles was smaller than a grid spacing (since the grid spacing represents the smallest resolution in our simulations, such a framework is reasonable for identifying particle clusters). For quantifying polymer-bridged clusters, the connectivity matrix was modified to account for binding between two particles to be defined when both are in contact with the monomers of the same polymer. A monomer was considered to be in contact with the particle when its distance from the surface of the particle is smaller than a grid space. To illustrate, SCMF simulation snapshots of PI1 particles and polymers forming direct particle aggregates and polymer-bridged particle aggregates are presented in Fig. 6.

Based on the above analysis, we quantify the number of clusters of size s (respectively identified for both direct particle–particle and polymer-bridged particle aggregates), denoted as $N(s)$. The fraction of the total number of particles forming a cluster of size s is denoted as $n(s)$ and is given as:

$$n(s) = \frac{sN(s)}{N_p}. \tag{14}$$

To distinguish between the two different kinds of clusters, *i.e.* the particle–particle (PP) and polymer-bridged particle (PB) aggregates, the cluster characteristics are denoted respectively as $n_p(s)$ and $n_{pol}(s)$.

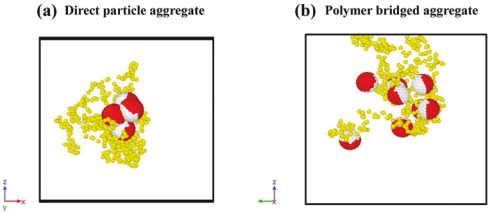

Fig. 6 SCMF snapshots of PI1 particles and polymers at ϕ_p = 0.10, C/C^* = 0.092 for (a) Q_{net} = 5: depicting direct particle aggregation; (b) Q_{net} = 40: depicting polymer-bridged particle aggregation.

4.4 Mixtures of homogeneously charged particles and polyanions

In our previous articles, we presented a comprehensive set of results for the structure and phase behavior of homogeneous positively charged particles.[20,51] Prior to discussing our results for heterogeneously charged particles, in this section we briefly summarize the results for the structure of both homogeneous positively and homogeneous negatively charged particles in polyanionic solutions for the parameters adopted for the present study.

In Fig. 7(a–d) we present the structural properties of homogeneous positively charged (solid lines) and negatively charged (dashed lines) particles in a negatively charged polymer solution. From the results displayed in Fig. 7(a), it is seen that for positively charged particles, the peak of the RDF is shifted from the particle surface. Such results are consistent with the observations presented in our earlier work,[20,51] wherein it was demonstrated that such parametric regimes lead to the formation of polymer-bridged clusters arising from polymer

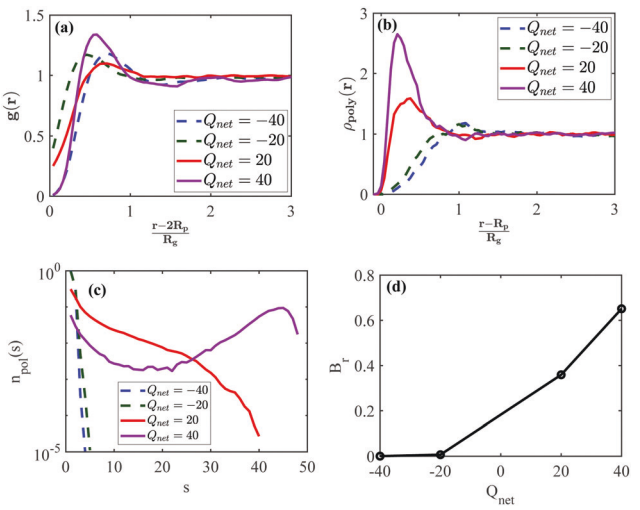

Fig. 7 (a) Particle–particle RDF; (b) normalized polymer concentration profile around the particle; (c) particle polymer cluster distribution; (d) bridging fraction. Q_{net} denotes the net charge of the particles. The results pertain to homogeneously charged particles (PI0) with particle volume fraction ϕ_p = 0.025 and polymer concentration C/C^* = 0.092.

adsorption on distinct, oppositely charged particles. Consistent with such a reasoning, the polymer density profiles displayed in Fig. 7(b) indicate polymer adsorption on positively charged particles. Moreover, supporting the polymer bridging hypothesis, the position of the RDF peak is seen to be relatively insensitive to the particle charge, and instead depending only on the polymer radius of gyration. Finally and more directly, the results depicted in Fig. 7(c) and (d) confirm the presence of polymer-bridged clusters with a significant fraction of polymers involved in bridging.

Interestingly, the results displayed in Fig. 7(a) for negatively charged particles exhibit characteristics which are similar to those seen for the positively charged particles. Specifically, a peak is seen in the RDF at a distance shifted from the surface of the particle. The origin of such a behavior is however distinct from the polymer-bridged structures seen for the positively charged particles. Specifically, for negatively charged particles, the polymers are expected to be depleted from the surface of the particle (Fig. 7(b)) due to a combination of the entropic costs arising from the exclusion from the particle interiors and the electrostatic repulsions arising from the like charges on the particles and the polymers. As a consequence, there is a polymer-induced attractive (depletion) interaction between the particles which competes with their direct electrostatic repulsions, and the structural characteristics that manifest represent an interplay of such interactions. Supporting such arguments, the position of the RDF peak is seen to shift further from the surface of the particle for $Q_{net} = -40$ (relative to $Q_{net} = -20$), due to the increased electrostatic repulsions. Moreover, it can indeed be seen that the polymer-bridged cluster characteristics displayed in Fig. 7(c) exhibit a monomer type distribution (involving less than 4–5 particles) for the negatively charged particles.

Together, the above results provide a framework to calibrate the results for polyampholyte particles presented in the following sections. Moreover, our observations also emphasize the need to utilize multiple characterization measures to unequivocally identify the structure of the polymer–particle mixtures.

4.5 Mixtures of polyanions and positive polyampholyte particles

In the present section, we discuss the results for the particle structural characteristics in mixtures of polyanions and positively charged polyampholyte particles. The results for the case of non-polyampholyte particles (in solutions of polyanions) were very similar to those observed for positive polyampholyte particles. Hence, we relegate the discussion of non-polyampholyte particles to the ESI.†

4.5.1 Influence of net charge, relative charge and pattern of charge inhomogeneities. To probe the effects of particle charge and heterogeneity on the resulting particle structural characteristics, we adopted a framework in which the net charge of particle ($Q_{net} = Q_p - Q_n$) was maintained fixed, while the ratio of Q_p to Q_n was modulated. Fig. 8(a–d) displays the results for $Q_{net} = 20$, and Fig. 8(e–h) presents the corresponding results for $Q_{net} = 40$. We first present results for the case of PI2 particles and subsequently compare the influence of different patterns of charge inhomogeneities.

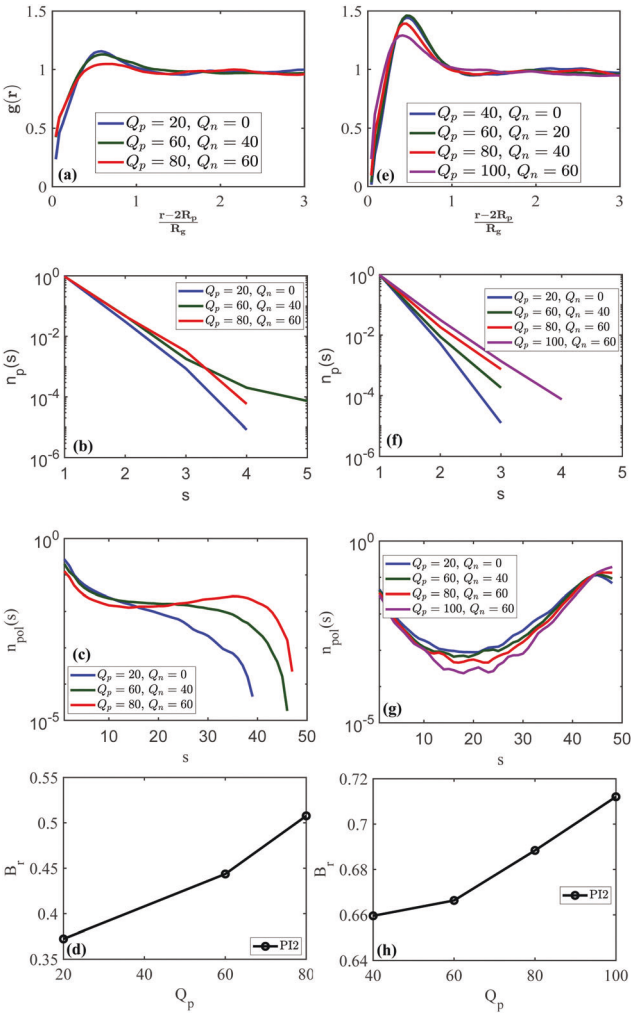

Fig. 8 Results for PI2 positive polyampholyte particles: (a) particle–particle RDF at different Q_p/Q_n for $Q_{net} = 20$; (b) size distribution of the particle–particle clusters for the system in (a); (c) size distribution of the particle–polymer clusters for the system in (a); (d) bridging fraction for the system in (a); (e) particle–particle RDF at different Q_p/Q_n for $Q_{net} = 40$; (f) size distribution of the particle–particle clusters for the system in (e); (g) size distribution of the particle–polymer clusters for the system in (e); (h) bridging fraction for the system in (e). For all the results, bulk polymer concentration $C/C^* = 0.092$, particle volume fraction $\phi_p = 0.025$.

We recall from the results discussed in Section 4.4 that in the case of positively charged homogeneous particles (PI0), an increase in the particle charge leads to an increase in both the intensity of the (polymer-bridged aggregate) peak in the RDF and the size of the polymer-bridged particle clusters (Fig. 7(a), (c) and (d)). Upon comparing the results for $Q_{net} = 20$ (Fig. 8(a–d)) with those for $Q_{net} = 40$ (Fig. 8(e–h)), we observe that positive polyampholyte particles exhibit trends which are consistent with such features, *viz.*, higher propensity for polymer-bridging and larger polymer-bridged clusters for the case of larger net particle charges.

Interestingly, in Fig. 8(a), (c), (d), (e), (g) and (h) we observe that an increase in the charge of the positive patches Q_p of the particles (for a fixed Q_{net}) simultaneously lowers the peak of the RDF and increases the polymer bridging fraction and the size of

the resulting polymer-bridged clusters. The lowering of the peak of the RDF can be understood as a consequence of the increase in the negative charge of the patches and the accompanying repulsion of the polymers from the particles, factors which can be expected to lower the interparticle bridging attractions. To understand the contrasting results observed in the polymer bridging fraction and the cluster sizes, we note that polyampholyte particles possess an additional source of electrostatic interparticle interaction arising from the presence of oppositely charged patches. The resulting attractive interactions are expected to be proportional to the product of the charge of individual patches, and hence become more significant for larger Q_p and Q_n. Such interactions counteract the electrostatic repulsions between the particles (arising from the same sign of the net charges), and is expected to bring the particles closer to each other. Such a hypothesis is supported by the increase in both the value of the RDF at particle contact (Fig. 8(a) and (e)) and the size of the particle–particle clusters (Fig. 8(b) and (f)) arising from an increase in Q_p. The influence of Q_p on the polymer-bridging and the polymer-bridged cluster characteristics can be ascribed to the closer proximity of the particles resulting from such electrostatic attractions.

Next, we consider the results for five different models of inhomogeneous charge distributions at a fixed volume fraction of the particles ϕ_p = 0.025, Q_p = 100 and Q_n = 60 (Q_{net} = 40). Fig. 9(a–d) present the particle–particle RDFs, sizes of particle–particle and particle–polymer clusters and the bridging fractions respectively.

From our discussion in the context of Fig. 8a, we recall that for Q_p = 40 and Q_n = 60, the particle structure for PI2 particles exhibited a peak in RDF corresponding to polymer-bridged aggregates. The results displayed in Fig. 9(a) indicate that the different patterns of charge inhomogeneities exhibit a very similar feature. However, in Fig. 9(a) we observe that the RDF value at particle contact decreases with an increase in the number of patches. Such a trend can be explained by the reasoning discussed above, *viz.*, that the positive polyampholyte particles experience an electrostatic attraction correlated with the product of the charges in the positive and negative patches. With an increase in the number of patches, the individual charge of the patches is correspondingly reduced (Q_p/n), leading to a decrease in the strength of the electrostatic attraction. Such a weakening of the electrostatic attractions, and the resulting larger interparticle distances, manifests as the smaller particle–particle (Fig. 9(b)) and polymer-bridged aggregates (Fig. 9(c)), and the lower bridging fractions observed for more patchier particles.

In summary, the results presented in this section demonstrate that positively charged polyampholyte particles form polymer-bridged particle clusters. The formation of such structures was more pronounced for larger net charge on the particle and for less patchier particles. With an increase in the charge of the positive patches, Q_p, and/or with a reduction in the patchiness of the particles, there was an increase in the size of polymer-bridged aggregates resulting from the closer proximity of the particles experiencing enhanced electrostatic attraction between the oppositely charged patches.

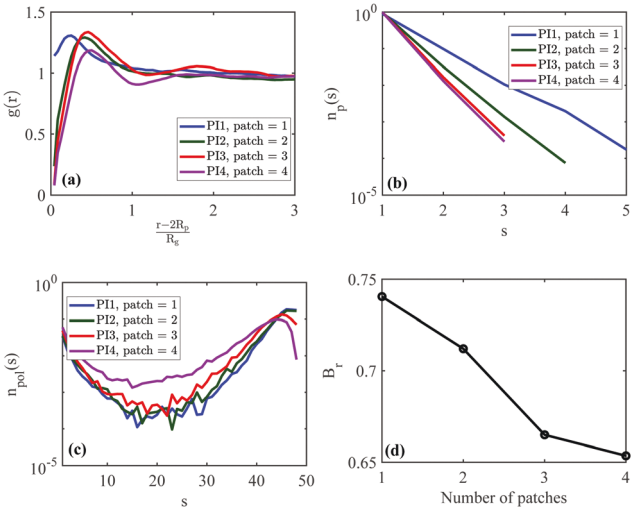

Fig. 9 (a) Particle–particle RDF at different charge distributions of positive-polyampholyte particles; (b) size distribution of the particle–particle clusters for the system in (a); (c) size distribution of the particle–polymer clusters for the system in (a); (d) bridging fractions as a function of the number of patches. For all the results, bulk polymer concentration C/C^* = 0.092, particle volume fraction ϕ_p = 0.025, Q_p = 100 and Q_n = 60.

4.5.2 Effects of particle volume fraction. Fig. 10(a–d) present results for the influence of particle volume fraction on the structure of PI1 and PI2 particles at a fixed particle charge Q_p = 80 and Q_n = 60. For all particle volume fractions ϕ_p, the particle structure for both PI1 and PI2 particles is seen to exhibit a weak peak in the RDF corresponding to polymer-bridged aggregates (Fig. 10(a)). With an increase in particle volume fraction, an increase is however seen in the contact value of the particle–particle RDF. Such trends are seen more prominently in PI1 particles, which exhibit a sharp peak at particle contact (in addition to the weak peak from polymer-bridged structures) for ϕ_p = 0.157. The above results are indicative of a transformation from polymer-bridged clusters with separated particles into direct particle aggregates. Supporting such a hypothesis, the particle–particle cluster size distributions (Fig. 10(a)) display a shift towards larger cluster sizes. As a consequence of the closer proximities of the particles due to such an aggregation (and the reduction in the average interparticle spacing resulting from increased number of particles), both the polymer-bridged clusters and the bridging fractions are also seen to shift to larger values with increasing particle volume fractions.

The above results can be understood to arise as a consequence of the screening-induced reduction in interparticle electrostatic repulsions. Indeed, in our earlier work,[51] we demonstrated that an increase in the particle volume fraction had an effect similar to an enhancement of depletion attractions which result from increasing polymer concentrations. Due to such a reduction in the interparticle electrostatic repulsions, both the direct attractions between the oppositely charged patches on the particles and the polymer depletion induced attraction become more relevant, leading to the formation of direct particle aggregates. To explain the influence of the pattern of charge inhomogeneity on such results, we again invoke the fact that the PI1 particles

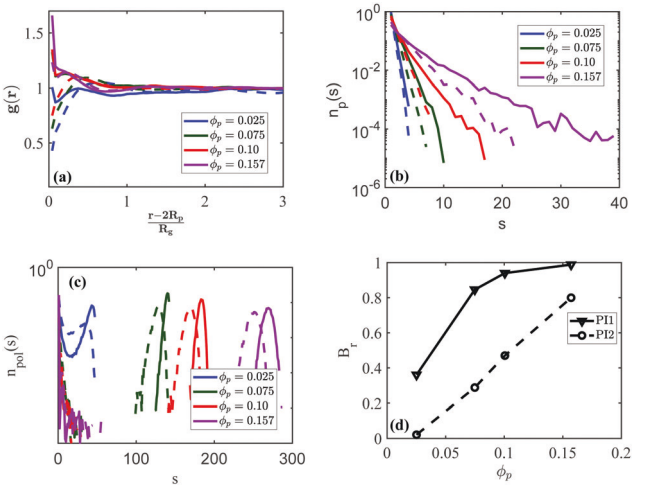

Fig. 10 Effect of particle volume fraction for positive polyampholyte particles: (a) particle–particle RDF; (b) particle–particle cluster distribution; (c) particle–polymer cluster distribution; (d) bridging fraction for different values of Q_p. For all the above results, Q_{net} = 20 with Q_p = 80 and Q_n = 60, C/C^* = 0.092. Solid lines are results for PI1 particles and dashed lines are for PI2 particles.

possess greater charge on the individual patches, and hence the direct electrostatic attractions which drive the particle clustering phenomena are expected to be stronger in such cases.

Based on the classification of the phases described in Section 4.3, we collated our results for positive polyampholyte particles in terms of "phase diagrams" (Fig. 11) which summarize our findings. Overall, it can be seen that increasing the charge on the positive patches and/or the particle volume fractions leads to an increased tendency to form particle aggregates. Upon comparing the different patterns of charge inhomogeneities, we observe that increasing the number of patches (for fixed Q_p and Q_n) has an effect similar to that of reducing the charge on the positive patches.

4.6 Mixtures of polyanions and negative polyampholyte particles

In this section we consider the particle structure and cluster characteristics for polyampholyte particles in which the net charge is negative (same as that of the polyanion).

4.6.1 Effect of net charge, relative charge and pattern of charge inhomogeneities. Similar to our discussions for the positive polyampholyte case, to unravel the effect of charge heterogeneities for net negatively charged polyampholyte particles, we maintained a fixed charge of the particle and varied the ratio of Q_p/Q_n to probe its effect on the structural properties of PI1 and PI2 particles (we present a discussion elaborating the influence of the pattern of charge inhomogeneities subsequently). Fig. 12(a–d) represent the results for particle–particle RDFs, particle–particle cluster distribution, particle–polymer cluster distribution and bridging fractions at a constant particle volume fraction ϕ_p = 0.025 and net charge of the particle Q_{net} = −40.

Fig. 12(a) presents the results for particle–particle RDFs. For lower values of Q_p (or Q_n), the RDFs exhibit characteristics of a

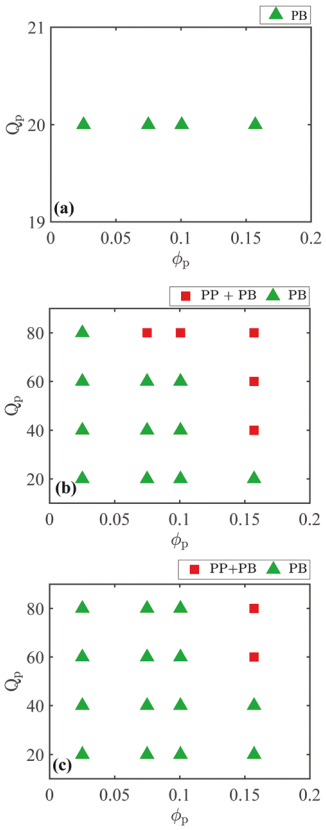

Fig. 11 Morphology based phase diagrams for positive polyampholyte particles: (a) PI0; (b) PI1; and (c) PI2 particles; for all the results, bulk polymer concentration C/C^* = 0.092. The net charge of all the particles is Q_{net} = 20 and $Q_n = Q_{net} - Q_p$. PP – direct particle aggregation; PB – polymer bridged aggregation; PP + PB – mixed phase.

dispersed phase for both PI1 and PI2 particles. In Section 4.4, for PI0 (homogeneous) negatively charged particles, it was seen that the RDF displayed a shifted peak from the particle surface (Fig. 7). Such characteristics were rationalized as arising from a combination of polymer depletion attractions and interparticle electrostatic repulsions. The results displayed in Fig. 12(a) contrast with such characteristics and demonstrate that simply rendering the particle charges inhomogeneous reduces both the extent of electrostatically driven polymer depletion and the resulting attractive interactions to an extent to eliminate the clustering characteristics seen for homogeneously charged particles.

With increasing Q_p and Q_n, the RDF value at the particle contact increases, leading to more pronounced particle–particle clusters (Fig. 12(b)), polymer-bridged clusters (Fig. 12(c)) and polymer bridging fractions (Fig. 12(d)). Such trends can be rationalized by a reasoning similar to that advanced in the context of positive polyampholyte particles, in which the increase in Q_p leads to a greater degree of electrostatic attraction between the oppositely charged patches, which in turn drives the formation of particle aggregates. The formation of such particle–particle clusters brings the particles into closer proximity, which enhances the formation of polymer bridges and the associated cluster sizes.

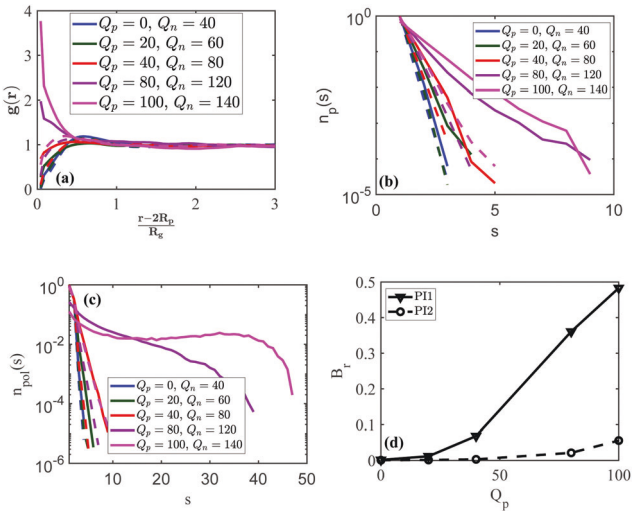

Fig. 12 Structure of negative-polyampholyte particles: (a) particle–particle RDF at different Q_p, Q_n; (b) size distribution of the particle–particle clusters for the system; (c) size distribution of the particle–polymer clusters; (d) bridging fraction. The results displayed correspond to net charge $Q_{net} = -40$, particle volume fraction $\phi_p = 0.025$, $C/C^* = 0.092$. Solid lines are results for PI1 particles and dashed ones are for PI2 particles.

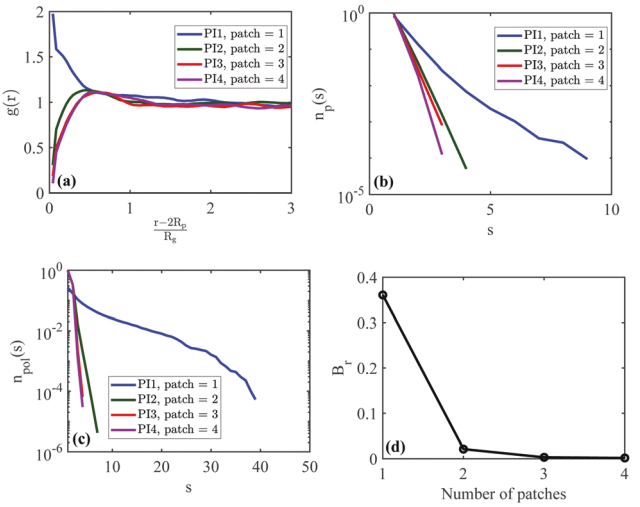

Fig. 13 Structure of negative-polyampholyte particles for different patterns of charge inhomogeneities: (a) particle–particle RDF; (b) size distribution of the particle–particle clusters; (c) size distribution of the particle–polymer clusters; (d) bridging fraction. The results displayed correspond to $Q_p = 80$, $Q_n = 120$, $C/C^* = 0.092$ and $Q_{pol} = -120$.

Fig. 13(a–d) present results for the influence of particle charge heterogeneity on the structure of negatively charged polyampholyte particles. For PI1 particles, the RDF is seen to exhibit a peak at particle contact. With an increase in the number of patches, the value of the RDF at contact is seen to decrease. Consistent with RDF results, the particle–particle cluster sizes (Fig. 13(b)) also increase with a decrease in the number of patches. Accompanying the formation of particle–particle clusters, the PI1 particles are also seen to exhibit substantial polymer bridging (Fig. 13(c) and (d)).

The above results are very similar to the trends observed in the context of positive polyampholyte particles (Fig. 9) and can again be rationalized based on the charge on the respective patches. More explicitly, an increase in the number of patches reduces the effective (positive and negative) charge on the patches, and thereby diminishes the direct electrostatic attractions. Moreover, the lowering of the charges also reduces the electrostatic polymer depletion and the resulting interparticle attractions. Together, such effects lead to an overall reduction in the particle aggregation and clustering phenomena.

In summary, the results presented in this section share a number of similarities in physics and outcomes to the results discussed in the context of positive polyampholyte particles. Mainly, we observe that an increase in the charge on the patches (at a fixed net charge of the particle) and/or a reduction in the number of patches leads to an increase in the tendency to form direct particle aggregates. However, it is of interest to note that polymer-bridged clusters were only observed as accompanying direct particle aggregates. Such results contrast with those seen in the context of positive polyampholyte particles, wherein polymer-bridged aggregate structures were seen to form even in the absence of direct particle aggregates.

4.6.2 Effect of particle volume fraction. To probe the effect of particle volume fraction on the structural properties of negative polyampholyte particles, we fixed $Q_p = 40$ and $Q_n = 80$, and varied the particle volume fraction. Fig. 14(a) displays the particle–particle RDFs for PI1 and PI2 particles for different particle volume fractions. In all cases, there is observed to be a peak in the RDF at a location shifted from the particle contact. With an increase in particle volume fraction, the intensity of the peak increases and the location of the peak moves closer

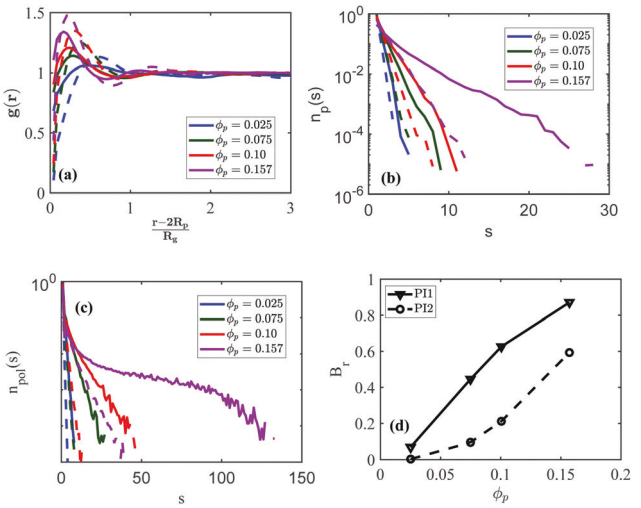

Fig. 14 Structure of negative-polyampholyte particles for different particle volume fractions: (a) particle–particle RDF at different ϕ_p for $Q_{net} = -40$; (b) size distribution of the particle–particle clusters for the system in (a); (c) size distribution of the particle–polymer clusters for the system in (a); (d) bridging fraction for the system in (a). For all, it is for polyampholyte patchy particles PI1 and PI2 with net charge $Q_{net} = -40$, $Q_p = 40$ and $Q_n = 80$, $C/C^* = 0.092$ and $Q_{pol} = 120$. Solid lines are results for PI1 particles and dashed ones are for PI2 particles.

to the particle surface. Consistent with such trends, both PI1 and PI2 particles are observed to form larger particle–particle clusters with an increase in particle volume fraction. Upon comparing PI1 and PI2 particles, we observe that the intensity of the peak is in general higher and the location is shifted further (from the particle surface) for PI1 particles.

To understand the above results, we point out the similarity between the general characteristics of the RDFs above and those discussed in the context of Fig. 7(a) in Section 4.4. Therein, the origin of the peak in the RDF was rationalized as arising from the combination of the interparticle electrostatic repulsions and the polymer depletion induced attractions. Further, we recall that the polymer depletion characteristics were also influenced by the electrostatic repulsion between the like-charged polymers and particles. Within such a framework, the results of Fig. 14(a) can be rationalized as arising from a similar interplay between electrostatic repulsions and depletion attractions. In such a context, the increase in the intensity and the shift in the location of the peak in the RDF with increasing particle volume fraction can be understood as a consequence of screening of electrostatic repulsions. Consistent with our hypothesis for the mechanism, and eliminating polymer-bridging interactions as a possible origin of the results, we observe that the polymer-bridged clusters encompass only a small fraction of particles for lower volume fractions (such results are to be contrasted with those seen in positively charged particles). At higher volume fractions, polymer-bridged clusters are seen to increase in size. However, such trends arise due to the increase in particle–particle clusters and the reduction in the average interparticle distances under such conditions.

Within the above framework, the differences observed between PI1 and PI2 particles can be rationalized based on the strength of electrostatic and depletion interactions which manifest in PI1 particles. Indeed, as discussed in earlier sections, PI1 particles possess larger magnitude of charges on the positive and negative patches. As a result, the direct electrostatic repulsions and the polymer depletion are expected to be stronger, which manifests in the intensity and the location of the peak in the RDF.

Similar to the results in Section 4.5.2, we collate all the results for the negatively charged polyampholyte particles in terms of a "phase diagram" for PI0, PI1 and PI2 particles for $Q_{net} = -40$. To describe the morphology, structures in which the peak of the RDF is shifted from the particle contact but exhibit only small particle–particle clusters are classified as dispersed phases. Structures in which the peak of the RDF is greater than unity and the particle–particle cluster sizes are greater than 10 are classified as particle–particle aggregates.

The results displayed in Fig. 15 are consistent with the earlier discussed observations. In general, we observe a propensity to form particle–particle aggregates more prevalent for particles with smaller number of patches and higher particle volume fractions. These are consistent with the strength of the electrostatic repulsions and the depletion interactions which manifest in such situations. Interestingly, none of the parameters we probed resulted in polymer-bridged aggregate phases in such negative polyampholyte particles. Such results and the contrast with experiments discussed in the introduction suggest that the partial dissociability of the proteins is likely an important factor in influencing such observations.

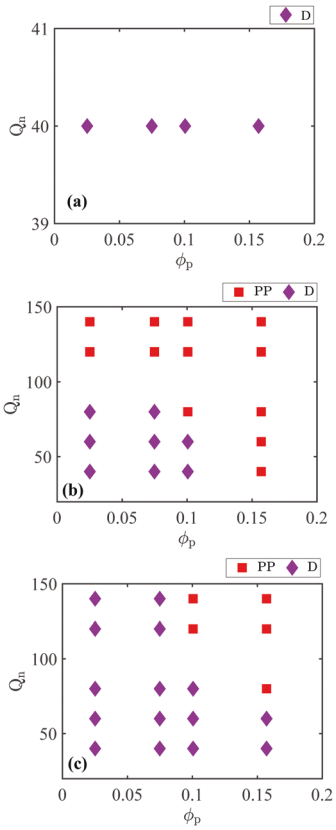

Fig. 15 Phase diagram for (a) PI0 (b) PI1 and (c) PI2 particles; for all the results, bulk polymer concentration $C/C^* = 0.092$. The net charge of all the particles is $Q_{net} = -40$ and $Q_p = Q_{net} - Q_n$. PP – direct particle aggregation; D – dispersed phase.

5 Summary

In this article, we have presented results for the effect of particle charge inhomogeneities on the structure and phase behavior in mixtures of nanoparticles and charged polyelectrolytes. We probed two classes of polyampholyte systems: (I) particles with a net positive charge and (II) particles with a net negative charge. For both the systems, we have studied the effect of geometry of charge distribution, the magnitude of positive charge (Q_p) and the particle volume fraction (ϕ_p).

For positive polyampholyte cases, the particles were seen to form either polymer-bridged or direct particle aggregates. Increasing the charge on the positive patches and/or the particle volume fractions leads to an increased tendency to form particle aggregates. Upon comparing the different patterns of charge inhomogeneities, we observe that increasing the number of patches (for fixed Q_p and Q_n) had an effect similar to that of reducing the charge on the positive patches. For negative

polyampholyte particles, we observed only direct particle aggregates. The propensity to form such structures was more prevalent for particles with smaller number of patches and higher particle volume fractions.

The results presented in the present article constitute the first steps towards addressing the influence of protein charge heterogeneities on the structure of protein–polyelectrolyte mixtures. A number of directions emerge for potential future studies. The primary among these is the inclusion of pH and partial dissociability effects of the charged groups. A second direction is the study of more realistic models for protein charge heterogeneities which may draw on the structures available in the protein data bank.

Conflicts of interest

There are no conflicts to declare.

Acknowledgements

We are grateful to Prof. Bradley Olsen for discussions which motivated this work. We also thank Justin Leung for performing some of the simulations on polyampholyte particles. We acknowledge funding in part by grants from the Robert A. Welch Foundation (Grant F1599), the National Science Foundation (DMR-1721512), King Abdullah University of Science and Technology (OSR-2016-CRG5-2993-1). Acknowledgment is also made to the Donors of the American Chemical Society Petroleum Research Fund for partial support of this research (56715-ND9). We acknowledge the Texas Advanced Computing Center (TACC) at The University of Texas at Austin for computing resources that contributed to the research results reported within this paper.

References

1 C. Schmitt and S. L. Turgeon, *Adv. Colloid Interface Sci.*, 2011, **167**, 63–70.
2 S. Dumitriu and E. Chornet, *Adv. Drug Delivery Rev.*, 1998, **31**, 223–246.
3 B. Kim, C. N. Lam and B. D. Olsen, *Macromolecules*, 2012, **45**, 4572–4580.
4 I. K. Voets, A. de Keizer and M. A. C. Stuart, *Adv. Colloid Interface Sci.*, 2009, **147-148**, 300–318.
5 J. S. Mohammed, M. A. DeCoster and M. J. McShane, *Biomacromolecules*, 2004, **5**, 1745–1755.
6 P. L. Dubin, J. Gao and K. Mattison, *Sep. Purif. Methods*, 1994, **23**, 1–16.
7 Y.-f. Wang, J. Y. Gao and P. L. Dubin, *Biotechnol. Prog.*, 1996, **12**, 356–362.
8 Y. Xu, M. Mazzawi, K. Chen, L. Sun and P. L. Dubin, *Biomacromolecules*, 2011, **12**, 1512–1522.
9 Y. Xu, M. Liu, M. Faisal, Y. Si and Y. Guo, *Adv. Colloid Interface Sci.*, 2017, **239**, 158–167.
10 B. de Jong, *Crystallisation- Coacervation- Flocculation*, Elsevier Publishing Company, 1949, vol. II.
11 H. Morawetx and J. W. L. Hughes, *J. Phys. Chem.*, 1952, **56**, 64–69.
12 F. Comert, A. J. Malanowski, F. Azarikia and P. L. Dubin, *Soft Matter*, 2016, **12**, 4154–4161.
13 C. G. de Kruif, F. Weinbreck and R. de Vries, *Curr. Opin. Colloid Interface Sci.*, 2004, **9**, 340–349.
14 R. Tuinier, J. Rieger and C. de Kruif, *Adv. Colloid Interface Sci.*, 2003, **103**, 1–31.
15 C. S. Cummings and A. C. Obermeyer, *Biochemistry*, 2018, **57**, 314–323.
16 A. B. Kayitmazer, *Adv. Colloid Interface Sci.*, 2017, **239**, 169–177.
17 W. B. Russel, D. A. Saville and W. R. Schowalter, *Colloidal Dispersions*, Cambridge University Press, 1989, vol. 54, pp. 201–202.
18 F. Carlsson, P. Linse and M. Malmsten, *J. Phys. Chem. B*, 2001, **105**, 9040–9049.
19 M. Skepö and P. Linse, *Phys. Rev. A: At., Mol., Opt. Phys.*, 2002, **66**, 051807.
20 G. Pandav, V. Pryamitsyn, J. Errington and V. Ganesan, *J. Phys. Chem. B*, 2015, **119**, 14536–14550.
21 E. Kizilay, A. B. Kayitmazer and P. L. Dubin, *Adv. Colloid Interface Sci.*, 2011, **167**, 24–37.
22 A. B. Kayitmazer, B. Quinn, K. Kimura, G. L. Ryan, A. J. Tate, D. A. Pink and P. L. Dubin, *Biomacromolecules*, 2010, **11**, 3325–3331.
23 K. Laos, G. J. Brownsey and S. G. Ring, *Carbohydr. Polym.*, 2007, **67**, 116–123.
24 F. L. B. da Silva and B. Jonsson, *Soft Matter*, 2009, **5**, 2862–2868.
25 Y. Li, Q. Zhao and Q. Huang, *Carbohydr. Polym.*, 2014, **101**, 544–553.
26 T. Harnsilawat, R. Pongsawatmanit and D. J. McClements, *Biomacromolecules*, 2006, **7**, 2052–2058.
27 K. W. Mattison, I. J. Brittain and P. L. Dubin, *Biotechnol. Prog.*, 1995, **11**, 632–637.
28 Y. Tsang and T. E. Thompson, *J. Phys. Chem.*, 1965, **69**, 4242–4249.
29 B. Hofstee, *Biochim. Biophys. Acta*, 1964, **91**, 340–343.
30 V. Lesins and E. Ruckenstein, *Colloid Polym. Sci.*, 1988, **266**, 1187–1190.
31 W. Kopaciewicz, M. Rounds, J. Fausnaugh and F. Regnier, *J. Chromatogr. A*, 1983, **266**, 3–21.
32 R. de Vries, F. Weinbreck and C. G. de Kruif, *J. Phys. Chem.*, 2003, **118**, 4649–4659.
33 R. de Vries, *J. Phys. Chem.*, 2004, **120**, 3475–3481.
34 M. Ellis, C. Y. Kong and M. Muthukumar, *J. Phys. Chem.*, 2000, **112**, 8723–8729.
35 Z. Zhang and S. C. Glotzer, *Nano Lett.*, 2004, **4**, 1407–1413.
36 N. Kern and D. Frenkel, *J. Phys. Chem.*, 2003, **118**, 9882–9889.
37 P. Teixeira and J. Tavares, *Curr. Opin. Colloid Interface Sci.*, 2017, **30**, 16–24.
38 E. Bianchi, G. Kahl and C. N. Likos, *Soft Matter*, 2011, **7**, 8313–8323.
39 E. Bianchi, R. Blaak and C. N. Likos, *Phys. Chem. Chem. Phys.*, 2011, **13**, 6397–6410.

40 G. Doppelbauer, E. G. Noya, E. Bianchi and G. Kahl, *Soft Matter*, 2012, **8**, 7768–7772.
41 J. P. K. Doye, A. A. Louis, I.-C. Lin, L. R. Allen, E. G. Noya, A. W. Wilber, H. C. Kok and R. Lyus, *Phys. Chem. Chem. Phys.*, 2007, **9**, 2197–2205.
42 E. Bianchi, C. N. Likos and G. Kahl, *ACS Nano*, 2013, **7**, 4657–4667.
43 E. Bianchi, C. N. Likos and G. Kahl, *Nano Lett.*, 2014, **14**, 3412–3418.
44 E. Bianchi, in *Modeling the Effective Interactions Between Heterogeneously Charged Colloids to Design Responsive Self-assembled Materials*, ed. I. Coluzza, *Springer International Publishing, Cham*, 2017, pp. 47–70.
45 A. C. Obermeyer, C. E. Mills, X.-H. Dong, R. J. Flores and B. D. Olsen, *Soft Matter*, 2016, **12**, 3570–3581.
46 M. Doi and S. Edwards, *The Theory of Polymer Dynamics*, A Clarendon Press Publication, 1988.
47 G. H. Fredrickson, *The equillibrium theory of inhomogenous polymers*, Oxford science publications, 2006.
48 K. C. Daoulas and M. Müller, *J. Phys. Chem.*, 2006, **125**, 184904.
49 F. A. Detcheverry, H. Kang, K. C. Daoulas, M. Müller, P. F. Nealey and J. J. de Pablo, *Macromolecules*, 2008, **41**, 4989–5001.
50 M. Müller and K. C. Daoulas, *J. Phys. Chem.*, 2008, **128**, 024903.
51 G. Pandav, V. Pryamitsyn and V. Ganesan, 2015.
52 N. Metropolis, A. W. Rosenbluth, M. N. Rosenbluth, A. H. Teller and E. Teller, *J. Phys. Chem.*, 1953, **21**, 1087–1092.
53 V. Pryamitsyn and V. Ganesan, *J. Phys. Chem.*, 2015, **143**, 164904.
54 V. Pryamitsyn and V. Ganesan, *Macromolecules*, 2014, **47**, 6095–6112.
55 R. Samanta and V. Ganesan, *Soft Matter*, 2018, **14**, 3748–3759.
56 V. Pryamitsyn and V. Ganesan, *J. Phys. Chem.*, 2013, **138**, 234905.
57 J. Koski, H. Chao and R. A. Riggleman, *J. Phys. Chem.*, 2013, **139**, 244911.
58 H. Chao, J. Koski and R. A. Riggleman, *Soft Matter*, 2017, **13**, 239–249.
59 E. M. Sevick, P. A. Monson and J. M. Ottino, *J. Phys. Chem.*, 1988, **88**, 1198–1206.
60 M. Surve, V. Pryamitsyn and V. Ganesan, *J. Phys. Chem.*, 2006, **125**, 064903.
61 M. Surve, V. Pryamitsyn and V. Ganesan, *Phys. Rev. Lett.*, 2006, **96**, 177805.
62 P. D. Godfrin, R. Castañeda-Priego, Y. Liu and N. J. Wagner, *J. Phys. Chem.*, 2013, **139**, 154904.

